Jomard Publishing

SYNTHESIS AND PROPERTIES OF SPINEL PHASES OF THE COMPOSITION $Ho_xPr_xMg_{1-2x}Al_2O_4$

Natavan Makhmudova[*], Teymur Ilyasly, Sabit Mammadov, Rena Abbasova

Department of General and Inorganic Chemistry, Baku State University, Baku, Azerbaijan

Abstract. Samples of spinel type $Ho_xPr_xMg_{1-2x}Al_2O_4$ were synthesized by low-temperature combustion. Temperatures of water release and weight loss were determined by thermogravimetric method. The phase composition and particle size of the samples were determined by X-ray phase analysis. The doping structure of $MgAl_2O_4$ spinel with Ho^{3+} and Pr^{3+}ions has been studied. It was found that doping with Pr^{3+} ions changes the color of the material from yellow to red. The color characteristics of spinel phase $HoPr:MgAl_2O_4$ doped simultaneously with holmium and praseodymium oxides were studied. Doping of the $Ho:MgA1_2O_4$ phase with praseodymium ions reduces the band gap of the obtained $HoPg:MgA1_2O_4$ crystals to 1.7 eV, and the absorption edge shifts towards red. The color characteristics of some doped spinel crystalline powders annealed at 800, 1000 and 1200°C for 3 hours showed that the color of the samples corresponds to values between the a* parameter (yellow color) and the b* parameter (red color). Relationships between the color parameters (a* and b*), the band gap, and the annealing temperature for the $Ho_{0.05}Pr_{0.05}Mg_{0.9}Al_2O_4$ and $Ho_{0.1}Pr_{0.1}Mg_{0.8}Al_2O_4$ compositions annealed at different temperatures were studied.

1. Introduction

Ceramic pigments have a mineral base (oxides, silicates, phosphates, metal tungstates) and are used for coloring, glazing, and decorating earthenware ceramics. They are very resistant to temperature changes, solar radiation, etc (Yungevis *et al.*, 2013; Vishnu *et al.*, 2011; Kumari *et al.*, 2012; Suzdalev *et al.*, 2006; Aruna *et al.*, 2008; Xiulan *et al.*, 2011). Unlike other pigments, ceramic pigments must form a low melting mixture for glazing. They are usually smaller (10-100 nm) than pigments for oil paints (0.5-1 microns). In relation to the glaze components, ceramic pigments are indifferent, do not enter into a chemical reaction with them impairing the color parameters (Belgin *et al.*, 2011; Cavalcante *et al.*, 2009; Costa *et al.*, 2008; Dondi *et al.*, 2006; Leila *et al.*, 2013; Trojan *et al.*, 1995).

Modern technology for the production of ceramic pigments is developing in several directions. The color parameters of pigments are improving. The resistance of pigments to the effects of temperature, radiation and sunlight is increasing. Their production cost is reducing. For many pigments, their color effect is due to the presence of chromophore elements. As chromophore elements, d-transition elements or rare earth elements are usually used. According to the origin of color, ceramic pigments are divided into: idiochromatic and allochromatic.

2. Experiments and results

The calculated stoichiometric amounts of metal nitrates are dissolved in distilled water in heat-resistant glasses, then heated on a hot plate with stirring to obtain a clear solution. The resulting solution is heated on a hot plate to a high temperature (150^0C) until water evaporates and powder is obtained. This powder is transferred to a muffle furnace, preheated to 350-400^0C. The powder ignites spontaneously at a certain temperature. The combustion reaction is completed within a few minutes and the ash obtained as a result of combustion in the form of a colored or colorless powder was subsequently used as a solid fuel. Fig. 1 shows a general scheme for the preparation of pigments and methods of analysis.
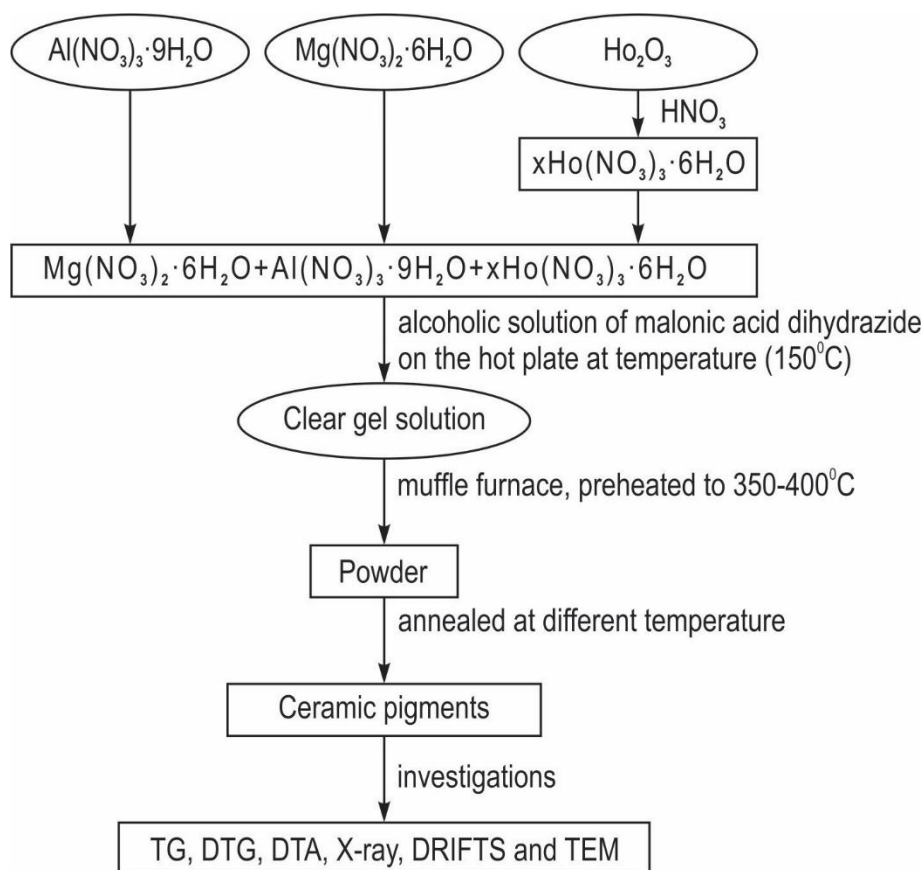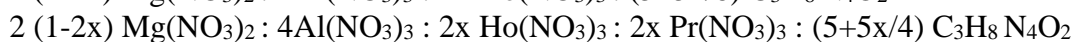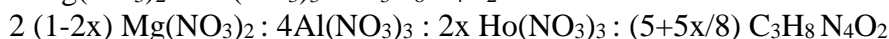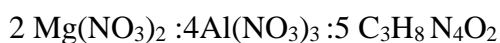

Figure 1. Scheme of preparation of pigments and methods of analysis

A solution of lanthanide nitrates was prepared by dissolving the calculated amounts of lanthanide oxides in nitric acid (65%) at a temperature of 50-60^0C, and solutions of 2 $Mg(NO_3)_2$ and $Al(NO_3)_3$ were prepared by dissolving salts in distilled water. At the second stage, nitrate solutions were mixed with an alcoholic solution of malonic acid dihydrazide at the ratios:

2 $Mg(NO_3)_2$: 4$Al(NO_3)_3$: 5 $C_3H_8N_4O_2$
2 (1-2x) $Mg(NO_3)_2$: 4$Al(NO_3)_3$: 2x $Ho(NO_3)_3$: (5+5x/8) $C_3H_8N_4O_2$
2 (1-2x) $Mg(NO_3)_2$: 4$Al(NO_3)_3$: 2x $Ho(NO_3)_3$: 2x $Pr(NO_3)_3$: (5+5x/4) $C_3H_8N_4O_2$

The taken amount of malonic acid dihydrazide was slightly (5%) bigger than stoichiometric. In the case of doping with two or three lanthanides, their sum of moles is Mx. When the prepared aqueous-alcoholic solutions are heated, the following reactions take place:

$$2Mg(NO_3)_2 \cdot 6H_2O + 4Al(NO_3)_3 \cdot 9H_2O + 5C_3H_8N_4O_2 \xrightarrow{300\,^\circ C} 2MgAl_2O_4 + 68\,H_2O + 15CO_2 + 18\,N_2$$

$$2(1-2x)Mg(NO_3)_2 \cdot 6H_2O + 4Al(NO_3)_3 \cdot 9H_2O + 2xHo(NO_3)_3 \cdot 6H_2O + (5+5x/8)C_3H_8N_4O_2 \xrightarrow{300\,^\circ C}$$

$$\xrightarrow{300\,^\circ C} 2Ho_xMg_{1-2x}Al_2O_4 + (68+5x/2)\,H_2O + (15+15x/8)\,CO_2 + (18+9x/4)\,N_2$$

$$2(1-2x)Mg(NO_3)_2 \cdot 6H_2O + 4Al(NO_3)_3 \cdot 9H_2O + 2x\,Ho(NO_3)_3 \cdot 6H_2O + 2xPr(NO_3)_3 \cdot 6H_2O +$$

$$(5+5x/4)\,C_3H_8N_4O_2 \xrightarrow{300\,^\circ C} 2Ho_xPr_xMg_{1-2x}Al_2O_4 + 68\,H_2O + (15+15x/4)\,CO_2 + (18+11x/2)N_2$$
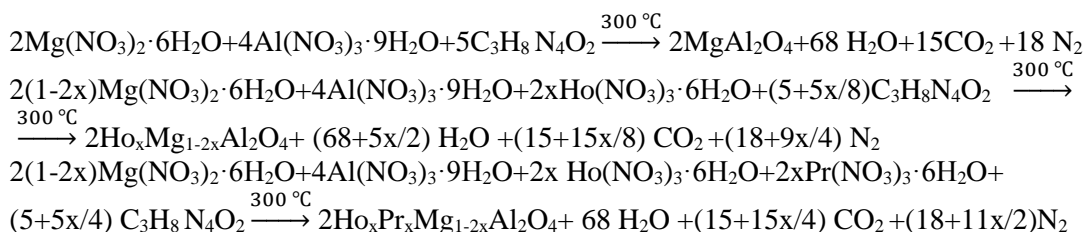
At this stage, an amorphous powder with a bulk composition of $MgAl_2O_4$, $Ho_xMg_{1-2x}Al_2O_4$ and $Ho_xPr_xMg_{1-2x}Al_2O_4$ is obtained. At the third stage, crystallization of amorphous powders occurs at 800, 1000, 1200^0C.

All samples for the study were prepared in the following way: at the same time, dihydrazide of malone complexes of all metals taken in stoichiometric amounts were mixed. In all cases, thermogravimetric curves of the prepared solid precursors (by evaporation) were recorded. According to the results of these curves, the course of synthesis was determined with further heating of the samples. The amount of samples for thermogravimetric analysis was about 100 mg. Based on thermogravimetric analysis, the temperature range of combustion and crystallization of amorphous substrates was determined.

Thermogravimetric analysis results are given as TG, DTG and DTA curves. The curves of thermogravimetric analysis of the sample with the composition $Ho_{0,1}Pr_{0,1}Mg_{0,8}Al_2O_4$ are shown in Fig. 2. As you can see from the figure, the TG curve (direct weight loss recording) consists of three sections. The first section includes the part of the curve corresponding to the temperature range of 80-300^0C. Here, the DTG and DTA curves show two endothermic effects at 1000 and 220-245^0C. The thermal effect at 100^0C is apparently associated with the presence of free water residues that remained in the samples after their evaporation, or again accumulates due to the hygroscopicity of the samples. The endothermic effect at 250^0C can be associated with the release of crystallization water. Here, the weight loss is only 7% of the original sample weight. It should be noted that the effects at 100 and 250^0C are also observed on the DTG curve of the $Ho_{0,1}Pr_{0,1}Mg_{0,8}Al_2O_4$ sample (Fig. 2). In the second section (temperature range 300-600^0C), the rate of weight loss slows down and, in this range, weight loss is 7 wt.%. In this temperature range, decomposition of the dry precursor occurs.

In the second section (temperature range 300-600^0C), the rate of weight loss slows down and, in this range, weight loss is 7 wt.%. In this temperature range, decomposition of the dry precursor occurs. A number of effects observed here on differential weight loss recording are associated with the release of combustion products (CO and CO_2) and possibly volatile decomposition components of the organic part of the substrate. In the third section, weight loss is 11 wt.% (600-900^0C) on the DTG curve at 675^0C, there is one deep effect with sharp intensity related to the weight loss of the sample. This can be explained by the final decomposition of the formed metal complexes of nitrate salts.
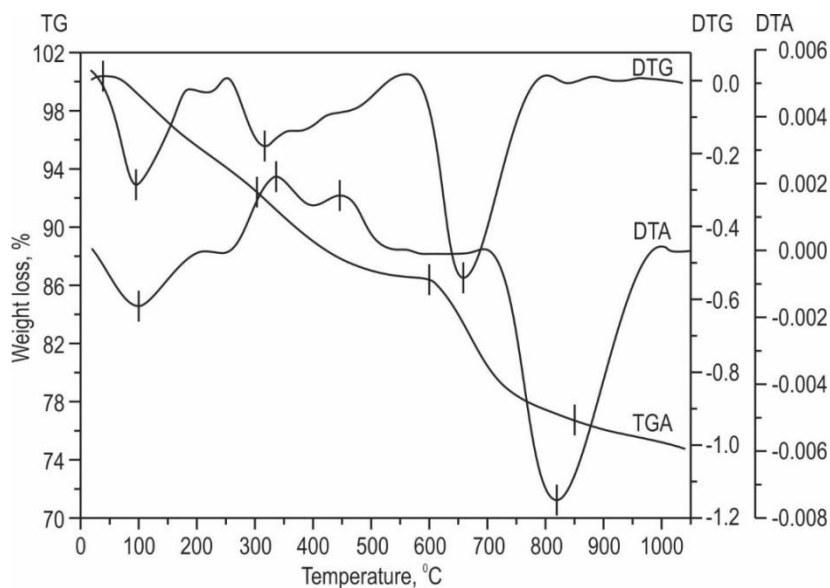
Figure 2. Results of thermogravimetric analysis (TG, DTG and DTA) of the synthesis of $Ho_{0,1}Pr_{0,1}Mg_{0,8}Al_2O_4$ and Ho_2O_3 powder from the dry residue

However, the latest version has not been confirmed, since the temperatures of thermal decomposition of nitric acid salts with the formation of NO do not correspond to the reality. Nitro groups can also be included in complex compounds after the primary combustion of the combustible part of the resulting complex with nitrate ligands. Interestingly enough, there is no deviation in the differential DTA notation next to this process. The deep endothermic effect on the DTA curve starts around 700°C with a center of effect at 840°C. Conversely, the slope of the TG curve decreases. We attributed this effect to the crystallization of an amorphous substrate. X-ray phase analysis of samples before and after 700^{0}C proves the progress of the crystallization process in this temperature range. And perfect crystals are obtained after a two-hour heat treatment of the samples above 800°C (Mann *et al.*, 1960; Patil *et al.*, 2008).

Diffraction patterns of samples of the composition $Ho_xPr_xMg_{1-2x}Al_2O_4$ are shown in Figure 2. They were removed from homogeneous powders, heat treated at 800, 1000 and 1200^{0}C for two hours. Heat treatment of the powders was carried out in muffle furnaces in the open air. The intensity of the X-ray reflections of the spinel phase increases with an increase in the annealing temperature and, at the same time, the width of the reflections narrows. The particle sizes were determined from the average width of X-ray reflections. Fig. 3 (d) shows the dependence of the nanoparticle size on the powder annealing temperature. As can be seen, the particle size increases with the heat treatment temperature (Mann *et al.*,, 1960; Patil *et al.*, 2008).

Fig. 3 (a, b) also shows the diffractograms of Ho_2O_3. The diffraction pattern of praseodymium oxide is identical to that of Ho_2O_3. Thus, the particles introduced into the composition of the rare earth elements occupy the cationic positions of the spinel structure, and some of them remain free in the form of mechanical mixtures. Free oxides form the known phase of the composition $Ho_{1-y}Pr_yO_{2-y/2}$ with a defective structure. The formation of this phase is confirmed by X-ray. The sizes of particles and phase composition, annealed at different temperatures, are established according to diffraction patterns. The results obtained are shown in Table 1.
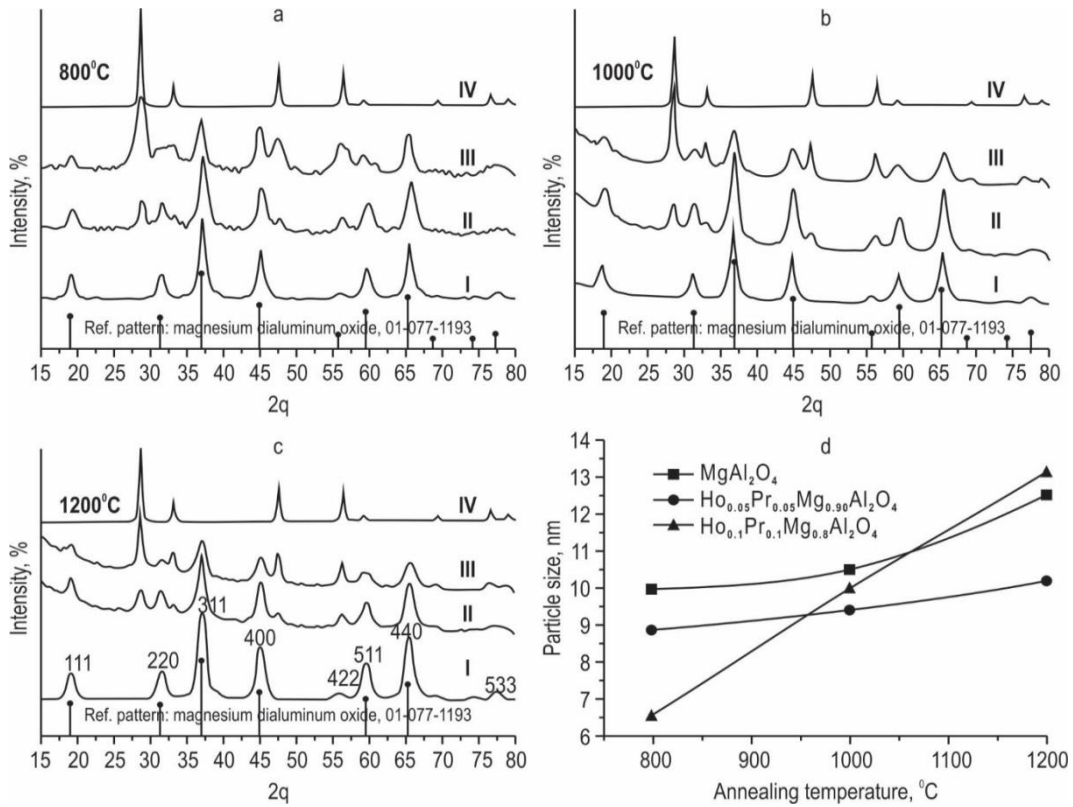
Figure 3. Diffractograms (a, b and c) I) Ho_2O_3, II) $MgAl_2O_4$, III) $Ho_{0.05}Pr_{0.05}Mg_{0.9}Al_2O_4$, IV) $Ho_{0.1}Pr_{0.1}Mg_{0.8}Al_2O_4$ and d) dependence of the particle size on the annealing temperature

Table 1. X-ray diffraction data of samples $MgAl_2O_4$, $Ho_{0.05}Pr_{0.05}Mg_{0.9}Al_2O_4$, $Ho_{0.1}Pr_{0.1}Mg_{0.8}Al_2O_4$ and Ho_2O_3, annealed at 800, 1000, and 1200°C

T, ^{0}C	Chemical composition	Particle size, nm	Phase composition	color
800	$MgAl_2O_4$	10	III	white
	$Ho_{0.05}Pr_{0.05}Mg_{0.9}Al_2O_4$	8.9	III + Ho_2O_3+PrO_2	orange
	$Ho_{0.1}Pr_{0.1}Mg_{0.8}Al_2O_4$	6.6	III + Ho_2O_3+PrO_2	orange
	Ho_2O_3	31	Ho_2O_3	yellow
1000	$MgAl_2O_4$,	10.5	III	white
	$Ho_{0.05}Pr_{0.05}Mg_{0.9}Al_2O_4$	9.4	III + Ho_2O_3+PrO_2	orange
	$Ho_{0.1}Pr_{0.1}Mg_{0.8}Al_2O_4$	10	III + Ho_2O_3+PrO_2	orange
	Ho_2O_3	32	Ho_2O_3	yellow
1200	$MgAl_2O_4$,	12.5	III	white
	$Ho_{0.05}Pr_{0.05}Mg_{0.9}Al_2O_4$	10.2	III + Ho_2O_3+PrO_2	orange
	$Ho_{0.1}Pr_{0.1}Mg_{0.8}Al_2O_4$	13.13	III + +PrO_2	orange
	Ho_2O_3	33	Ho_2O_3	yellow

The results of IR spectra for $Ho_xPr_xMg_{1-2x}Al_2O_4$ systems (where x = 0.00, 0.05, and 0.1) at different annealing temperatures are shown in Table 2. In 800-4000 cm^{-1} in the IR spectrum, the passbands at 3614-3400 cm^{-1} and 1647-1636 cm^{-1} for various systems at 300 and 1000°C can be associated with the presence of water or surface and free hydroxyl groups or crystalline water. The peak intensities at 2928-1428-1385-800 cm-1 can be obtained from fluctuations in CH, NO_3 or NO_x, which gradually decrease

with time. The observed passbands at 800-400 cm^{-1} can be associated with the amorphousness of the samples heated to 300°C. The transmission bands in the frequency range 706-459 cm^{-1} up to 1000°C correspond to the vibrational spectra of | MeO | bonds, and in spinel phases they are linked by the presence of coordination spheres octahedral | AlO_6 | and tetrahedral | MgO_4 | types.

Table 2. Passbands found in IR spectra heated to 300 and 1000°C

T,^{0}C	Systems	Anticipated groups, cm^{-1}			
		-OH	O-H	N=O	M-O
300	$MgA1_2O_4$,	3456	1636	1385-800	683-451
	$Ho_{0.05}Pr_{0.05}Mg_{0.9}Al_2O_4$	3614	1647	1404-800	687-490-417
	$Ho_{0.1}Pr_{0.1}Mg_{0.8}Al_2O_4$	3400	1639	1400	700-586-421
	Ho_2O_3	3429	1639	1400	650-529-430
1000	$MgA1_2O_4$,	3449	1639	1400	698-513
	$Ho_{0.05}Pr_{0.05}Mg_{0.9}Al_2O_4$	3425	1639	1400	702-560-494
	$Ho_{0.1}Pr_{0.1}Mg_{0.8}Al_2O_4$	3437	1639	1400	706-517-459
	Ho_2O_3	-	-	-	650-500-420

Fig. 4 (a and b) shows a TEM micrograph of samples of the composition $Ho_{0.1}Pr_{0.1}Mg_{0.8}Al_2O_4$ thermally treated at 1000°C. As you can see, they are flat and spherical. Fig. 4. b shows a histogram of particle size distribution. According to the TEM micrograph, the size of the samples varies from 7 to 14 nm. The average particle size is calculated by averaging about thirty particles. Particle measurement for $MgA1_2O_4$ is about 11 nm and 12 nm for $Ho_{0.1}Pr_{0.1}Mg_{0.8}Al_2O_4$. The particle sizes determined by TEM micrographs are in good agreement with the particle sizes determined from the diffractogram by the Scherer method.
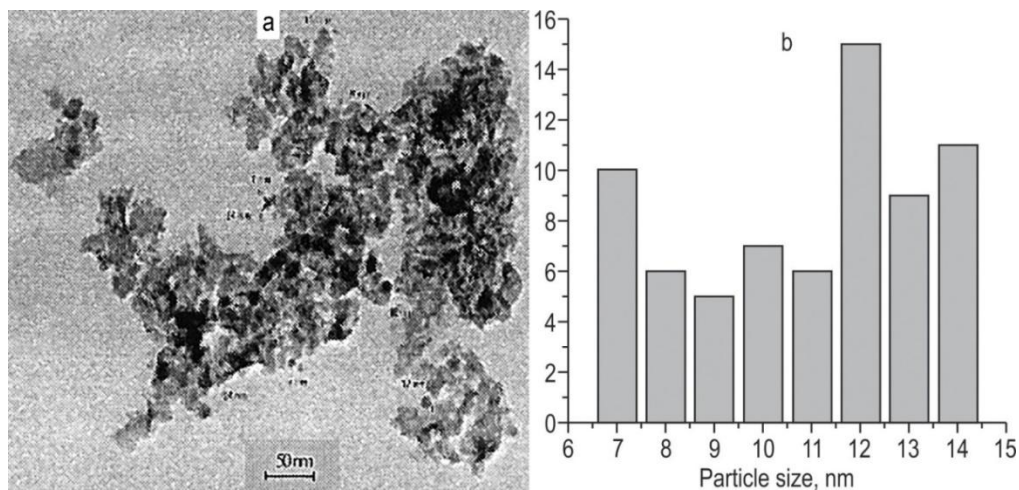

Figure 4. TEM microphotograph (a) and the number of particles of a certain size (b) for a $Ho_{0.1}Pr_{0.1}Mg_{0.8}Al_2O_4$ sample annealed at 1000°C

We took the diffuse reflectance spectra of pigment powders annealed at different temperatures shown in Fig. 5. The doping of the spinel structure $MgA1_2O_4$ with Ho^{3+} and Pr^{3+} oxide for the production of non-ferrous ceramic materials, $Ho_xPr_xMg_{1-2x}A1_2O_4$ ($MgA1_2O_4$ and $Ho_{1-y}Pr_yO_2$) has been studied. The light-yellow color of the additive from HoO_2 or a solid solution with $MgA1_2O_4$ as a result of the transition

transfers the charge between O_{2p} and Ho_{4f} (band gap = 2.76 eV). Doping of this system ($Ho_xMg_{1-x}Al_2O_4$) with Pr^{4+} ($4f^1$) gives an additional electron transferring charge between O_{2p} and Ho_{4f} in order to reduce the band gap from 2.76 to 1.7 eV.
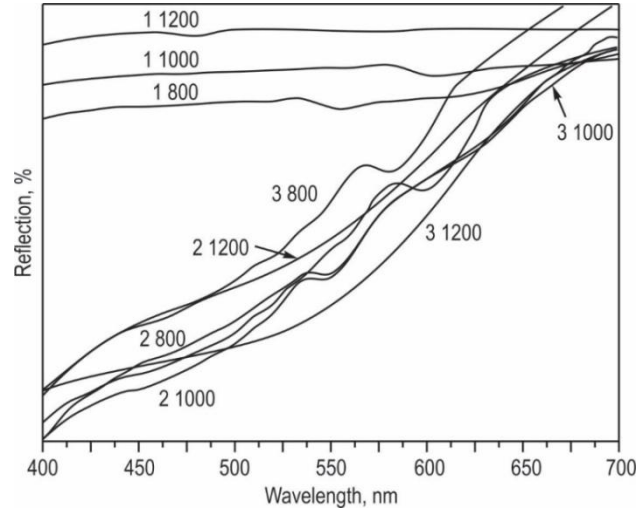

Figure 5. Diffuse reflectance spectra of 1) $MgAl_2O_4$, 2) $Ho_{0.05}Pr_{0.05}Mg_{0.9}Al_2O_4$ and 3) $Ho_{0.1}Pr_{0.1}Mg_{0.8}Al_2O_4$ of the samples annealed at 800, 1000, and 1200°C

Doping with Pr^{3+} ion changes the color of the material from yellow to red. We have studied the color changes of these compounds at different temperatures and the color parameters given in Table 3. The powder reflection diffusion spectra were recorded at the Ceramic Material Laboratory, Anadolu University, Turkey on a JASCO spectrometer in the visible region (400-700 nm).

Figure 5. shows the diffuse reflectance spectra of pure $MgAl_2O_4$ and doped crystals. The color characteristics of the spinel phases $HoPr:MgAl_2O_4$, simultaneously doped with holmium and praseodymium oxides, have been studied.

Additional doping of the $Ho:MgAlO_4$ phase with praseodymium ions reduces the band gap of the obtained $HoPr: MgAl_2O_4$ crystals to 1.7 eV (Fig. 6) (Ali *et al.*, 2013a,b,c; Ali *et al.*, 2012; Ibragimova *et al.*, 2013), and the absorption edge shifts towards the red color.

Table 3. Color characteristics for different samples annealed at 800, 1000 and 1200^{0}C for two hours

T, ^{0}C	Chemical composition	Color characteristics					Band gap, eV
		L^*	a^*	b^*	C^*	H^*	ΔE, эВ
800	$MgAl_2O_4$,	98,30	-0,16	0,34	0,38	64.8	3,76
	$Ho_{0.05}Pr_{0.05}Mg_{0.9}Al_2O_4$	88,20	2,37	6,35	6,77	69,5	2,10
	$Ho_{0.1}Pr_{0.1}Mg_{0.8}Al_2O_4$	76,50	6,10	9,71	11,50	57,86	1,88
1000	$MgAl_2O_4$,	97,97	-0,16	0,45	0,48	70,43	3,26
	$Ho_{0.05}Pr_{0.05}Mg_{0.9}Al_2O_4$	75,77	5,10	11,10	12,22	65,30	1,94
	$Ho_{0.1}Pr_{0.1}Mg_{0.8}Al_2O_4$	69,45	7,92	9,50	12,37	50,25	1,75
1200	$MgAl_2O_4$,	97,90	0,07	0,78	0,78	84,90	2,95
	$Ho_{0.05}Pr_{0.05}Mg_{0.9}Al_2O_4$	70,94	6,10	11,87	13,30	63,20	1,91
	$Ho_{0.1}Pr_{0.1}Mg_{0.8}Al_2O_4$	63,66	9,49	11,61	15,00	50,73	1,70

It was found that the addition of praseodymium as a doping element to the composition of additional ions, allows changing the color of the samples from yellow to red. In turn, the temperature and duration of heat treatment affects the color of the obtained sample. The color parameters of some alloyed crystalline spinel powders annealed at 800, 1000, and 1200°C for 3 hours are shown in Table 3.

The color of the samples appears between parameter a* (yellow) and parameter b* (red). This means that the color of the swatches is between red and yellow. The relationship between color parameters (a* and b*), bandgap and annealing temperature is shown in Figure 6. As can be seen from the figure, for the composition $Ho_{0.05}Pr_{0.05}Mg_{0.9}Al_2O_4$ and $Ho_{0.1}Pr_{0.1}Mg_{0.8}Al_2O_4$ annealed at different temperatures, the color parameter b* is greater than the color parameter a *. At the same time, a * and b* increase with decrease of the width of the forbidden samples and, at the same time, the color intensity increases.

As shown in Fig. 6.a the value of the color parameter b* is greater than the parameter a* and the difference between the parameter b* and a* is significant. This means that the color of the samples will be orange-yellow. As shown in Fig. 6, the parameter b* is larger than the parameter a* and the difference between them is small.
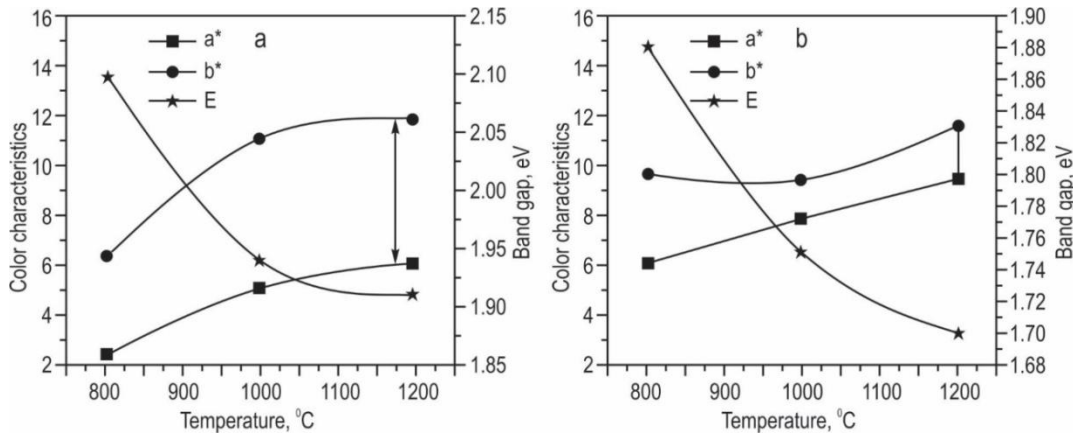

Figure 6. Changes in color parameters and band gap for a) $Ho_{0.05}Pr_{0.05}Mg_{0.9}Al_2O_4$ and b) $Ho_{0.1}Pr_{0.1}Mg_{0.8}Al_2O_4$ samples annealed at different temperatures

This means that the color of the samples should be red-orange. Color saturation or saturation C* increases with annealing at different temperatures and is in direct proportion to the amount of doping x and the chromaticity value presented in Table. 3.

H* angles color pigments observed in the yellow region of cylindrical color coordination $Ho_{0.05}Mg_{0.95}Al_2O_4$ and $Ho_{0.1}Mg_{0.9}Al_2O_4$ (standard value h*=70-105° for yellow) and in the orange region for $Ho_{0.05}Pr_{0.05}Mg_{0.9}Al_2O_4$ and $Ho_{0.1}Pr_{0.1}Mg_{0.8}Al_2O_4$ (standard value h *=35-70° for orange) and chromaticity values are presented in Table. 3.

This means that Pr doping shifts the color of the material from yellow to orange. Fig. 7 (a,b) shows UV-visible absorption spectra for the $Ho_{0.05}Pr_{0.05}Mg_{0.9}Al_2O_4$ and $Ho_{0.1}Pr_{0.1}Mg_{0.8}Al_2O_4$ samples annealed at 800, 1000, and 1200^0C. It is known that the absorption edge of pure $MgAl_2O_4$ depending on the heat treatment temperature is observed in the wavelength range of 330-420 nm (Fig. 7). Doping of holmium and praseodymium ions in the spinel structure changes the absorption edge and the width of the requested zone of the samples in the range 2.1-1.91eV for $Ho_{0.05}Pr_{0.05}Mg_{0.9}Al_2O_4$

and from 1.88-1.7eV for $Ho_{0.1}Pr_{0.1}Mg_{0.8}Al_2O_4$. Fig. 7.c shows the bandgap for $MgAl_2O_4$, $Ho_xMg_{1-x}Al_2O_4$ and $Ho_xPr_xMg_{1-2x}Al_2O_4$. The band gap of the $Ho_xPr_xMg_{1-2x}Al_2O_4$ phases decreases with an increase in the amount of alloying elements
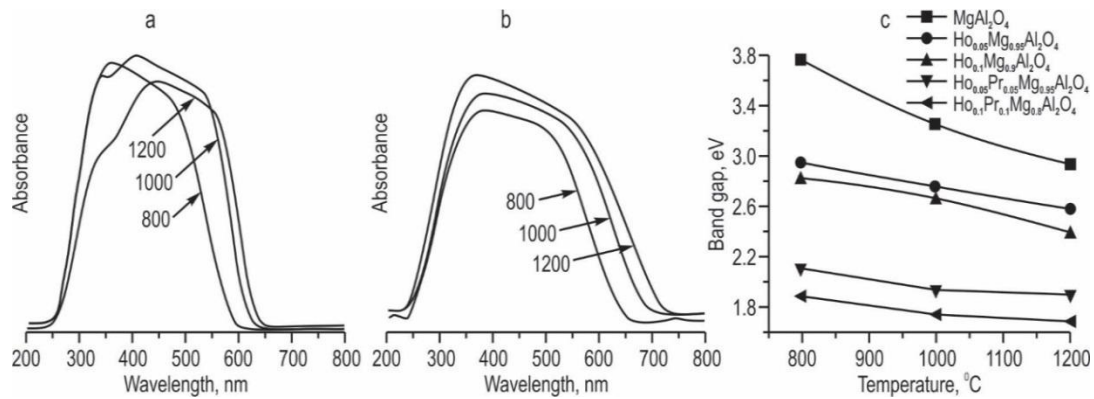

Figure 7. Absorption in the UV and visible spectral regions a)$Ho_{0.05}Pr_{0.05}Mg_{0.9}Al_2O_4$ b)$Ho_{0.1}Pr_{0.1}Mg_{0.8}Al_2O_4$ c)dependence of the band gap for samples thermally treated at 800,1000 and 1200°C

3. Conclusion

A method for the synthesis of spinel phases has been developed. It was found that the replacement of magnesium with a rare earth element (holmium and praseodymium) produces nanopowders of the composition $Ho_xPr_xMg_{1-2x}Al_2O_4$. Particle sizes were determined up to the average value of X-ray reflections. It was revealed that the particle size increases from the heat treatment temperature. It was revealed that the holmium-doped spinel $MgAl_2O_4$ phase lowers the band gap. Doping the material with Pr^{3+} shifts the color from yellow to orange.

References

Ali, A.A., Allazov, M., & Ilyasli, T. (2013a). Fabrication and study Tb3+: MgAl2O4 by combustion method using malonic acid dihydrazide as fuel. *International Journal of Advanced Scientific and Technical Research*, *1*(3), 358-367.

Ali, A.A. & Allazov, M.R., & Ilyasli, T.M. (2012*)*. Synthesis of $Pr_xMg_{1-2x}Al_2O_4$ (x=0-0,05-0,1) nanoparticle and study of their properties. *Azerbaijan Chemical Journal,* 4, 61-66.

Ali, A.A., Allazov, M.R., & Ilyasli, T.M. (2013b). Synthesis of spinel and its nanoparticles doped with rare earth elements by combustion. *11th All-Russian Youth Scientific Conference "Youth and Science in the North",* 4-5.

Ali, A.A., Karasu, B., Allazov, M.R., & Ilyasli, T.M. (2013c). Synthesis characterization and study of the effect of Yb^{3+} on $MgAl_2O_4$ spinel structure via combustion method. *Chemistry Journal, 3*(5), 133-138.

Aruna, S.T. Mukasyan, A.S. (2008). Combustion synthesis and nanomaterials. *Current Opinion in Solid State and Materials Science.* 12, 44-50.

Belgin, T., Servet T. (2011). Black ceramic pigments for porcelain tile bodies produced with chromiteores and iron oxide waste. *Journal of Ceramic Processing Research, 12(*4*),* 462-467.

Cavalcante, P.M.T., Dondi, M., Guarini, G., Raimondo, M., & Baldi, G. (2009). Colour Performance of Ceramic nano-pigments. Dyes and Pigments, 80, 226-232.

Costa, G., Dela, V.P, Ribeiro, M.J., Oliveria, A.P.N., Monros, G. & Labrincha, J.A. (2008). Synthesis of black ceramic pigments from secondary raw materials. *Dyes Pigments*, 77,

137-144.

Cox, J.D. & Pilcher G. (1970). Thermochemistry of organic and organometallic Compounds. *Academic Press, New York,* 631-636.

Dondi, M., Matteucci, F., & Cruciani G. (2006). Zirconium titante ceramic pigments: crystal structure, optical spectroscopy and texnological properties. *J. Soid State Chem., 179*(1), 233-246.

Ibragimova, F.S., Mammadov, S.Q, Ali, A.A., Allazov, M.R., & Ilyasli, T.M. (2013). Synthesis and study of Ce: $MgAl_2O_4$ spinel-structured nanoparticles. *The VI scientific conference of the doctoral candidates, masters and young researchers on the "Actual problems of chemistry", dedicated to the 89th anniversary of national leader Heydar Aliyev, Baku,* 122.

James, V., Prabhakar, Rao P., Sameera, S., & Divya S. (2014). Multiferroic based reddish brown pigments: $Bi_{1-x}M_xFeO_3$ for coloring applications. *Ceramics International, 40*(1), 2229-2235.

Kumari, L.S., Rao, P.P., Sameera, S., & Koshy, P. (2012). Synthesis and optical properties of $Ce_{0.95}Pr_{0.05-x}M_2O_2$ (M= Mn, Si) as potential ecological red pigments for coloration of plastics. *Ceramics International, 38,* 4009-4016.

Leila, T., Maryam, D. & Zahra B. (2013). Polymeric Precursor Route for the Synthesis of Nano sized $Co_xMg_{1-x}Al_2O_4$ Blue Pigments. *Middle-East Journal of Scientific Research, 14*(8), 1051- 1055.

Mann, F.G., Saunders, B.C. (1960). *Practical Organic*, Fourth edition, Longman Inc; New York, 117-119.

Patil, K.C., Hegde, M.S., Rattan, T., & Aruna S.T. (2008). *Chemistry of Combustion Synthesis, Properties and Applications: Nanocrystalline oxide Materials.* World Scientific publishing Co.Pte.Ltd., London, 335.

Suzdalev, I.P. (2006). *Nanotechnology: Physical Chemistry of Nanoclusters and Nanostructure of Nanomaterials*. Moscow, Kniga, 592.

Trojan, M., Sole, Z., Novotny, M., & Othmer, K. (1995). *Encyclopedia of Chem. Pigments, Techol*. New York: John Wiley and Sons Inc.

Vishnu, V.S., Reddy M.L. (2011). Near-infrared reflecting inorganic pigments based on molybdenum and praseodymium doped yttrium cerate: Synthesis, characterization and optical properties. *Solar Energy Materials & Solar Cells, 95,* 2685-2692.

Xiulan, D., Mei, P., Fapeng, Y., & Duorong, Y. (2011). Synthesis, strycture and optical properties of $CoAl_2O_4$ soinel nanocrystals. *J. of Alloy Compd., 509,* 1079-1083.

Yungevis, H., & Ozel, E. (2013). Effect of the milling process on the properties of $CoFe_2O_4$ pigment. *Ceramics International, 39*(5), 5503- 5511.